

Chaotic Free-Space Laser Communication over Turbulent Channel

N.F. Rulkov,¹ M.A. Vorontsov,² and L. Illing¹

¹*Institute for Nonlinear Science, University of California, San Diego, La Jolla, CA 92093*

²*Army Research Laboratory, Adelphi, Maryland 20783*

(Dated: March 30, 2022)

The dynamics of errors caused by atmospheric turbulence in a self-synchronizing chaos based communication system that stably transmits information over a ~ 5 km free-space laser link is studied experimentally. Binary information is transmitted using a chaotic sequence of short-term pulses as carrier. The information signal slightly shifts the chaotic time position of each pulse depending on the information bit. We report the results of an experimental analysis of the atmospheric turbulence in the channel and the impact of turbulence on the Bit-Error-Rate (BER) performance of this chaos based communication system.

PACS numbers: 05.45.Vx, 42.68.B, 42.60

Studies of chaos in nonlinear electrical circuits [1] and lasers [2] have shown that chaotic signals generated in these systems can potentially be used as carriers for information transmission. Thanks to the deterministic origin of chaos, two coupled chaotic systems can self-synchronize reproducing at the receiver end the chaotic waveforms generated in the transmitter [3]. This regime of self-synchronization is a key element in the recovery of information encoded in the received chaotic signal [4]. Due to the variety and complexity of the nonlinear dynamical issues involved, such chaos based communication systems are of broad interest both for theoreticians and experimentalists [5].

All practical communication channels introduce signal distortions that alter the chaotic waveform shape, as the result, the received chaotic oscillations do not precisely represent the transmitter oscillations. Channel noise, filtering, attenuation variability and other distortions in the channel corrupt the chaotic carrier and information signal. The presence of these channel distortions significantly hamper the onset of identical synchronization of the chaotic systems [6]. When signal distortions in the channel exceed a certain level, self-synchronizing fails resulting in failure of the communication link.

The enhanced sensitivity to chaotic signal waveform shape distortions and the resulting problems with chaos synchronization remain the major problems in the studies of chaos-based communications systems. In order to overcome the problems of channel distortions, a number of special chaotic communication methods have been proposed [7]. At least in theory and numerical simulations, it appears that the regime of identical synchronization in these specially designed systems is significantly less sensitive to channel noise and waveform distortions caused by limited bandwidth of the channel [8]. However, to the best of our knowledge, self-synchronizing chaos communication over a real-life highly non-stationary channel has not been demonstrated so far.

In this letter we report the experimental study of a chaotic self-synchronizing free-space laser communication

in the presence of severe communication signal distortions caused by atmospheric turbulence. Chaotic pulse signals were used as the optical communication carrier. Results demonstrate reliable self-synchronization of two coupled chaotic systems for most of the time and reveal the dynamical properties of errors bursts. Synchronization failed only when deep signal fading occurred so that the received power decreased to the photo-receiver noise level.

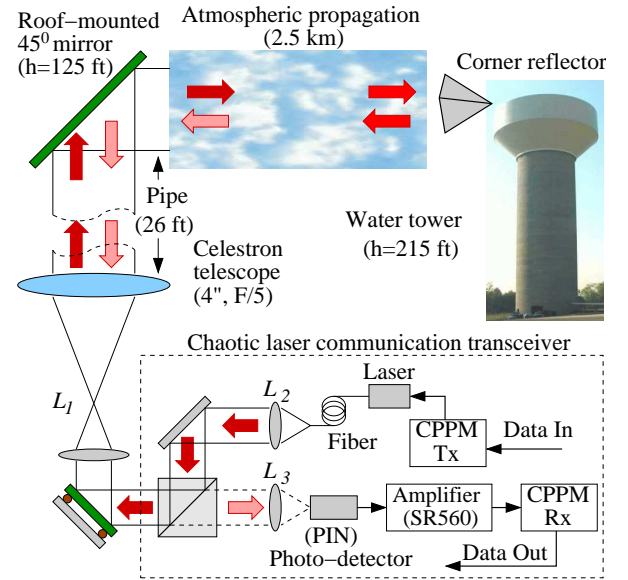


FIG. 1: Schematic for free-space laser communication system based on chaotic pulse position modulation transceiver.

A schematic representation of the chaotic free-space laser communication system used is shown in Fig. 1. The intensity-modulated 10 mW semiconductor laser beam ($\lambda = 690\text{nm}$) coupled to a single-mode fiber. Using a lens relay system (lenses L_1 and L_2) and the transmitter telescope (Celestron) the beam from the fiber was expanded to a 4 inch diameter. The laser beam propagation path included a 26 ft long vertical air-locked pipe

connecting the optical table with a 45° mirror placed inside a shed on the roof of the building, with subsequent propagation over an atmospheric path of length $L \simeq 2.5$ km. At the end of the propagation path was a $4''$ corner cube reflector placed on top of a water tower. After reflection the laser beam propagated from the water tower back to a communication receiver telescope in the roof-mounted shed. The receiver system used the same Celestron telescope and lens relay system (lenses L_1 and L_3) as did the transmitter system. The total double-pass atmospheric laser beam propagation distance was approximately $2L \simeq 5$ km long.

Double-pass wave propagation in a medium with random refractive index fluctuations displays interesting statistical properties known as backscatter enhancement. Backscatter enhancement results from correlations in the wavefront phase aberrations between the outgoing and returned waves which have propagated through the same refractive index inhomogeneities [9, 10]. The variance of the received wave phase and intensity fluctuation enhancement can exceed the corresponding value for a uni-directional wave that propagates the distance $z = 2L$ in an optically inhomogeneous medium. Under conditions of strong intensity fluctuations the backscatter enhancement factor can exceed a factor of two [11].

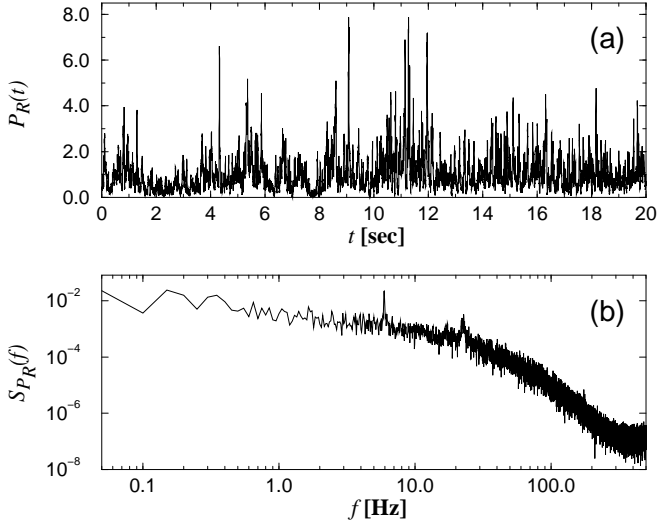


FIG. 2: Fluctuations of the received power $P(t)$ in the experiment with non-modulated laser generating constant output intensity (10mW). Normalized received power $P_R(t) = P(t)/\langle P(t) \rangle$ measured at the photo-detector output - (a), and corresponding averaged power spectrum of $P_R(t)$ - (b) illustrate the presence of strong laser beam intensity scintillations.

The received laser beam power was registered by the PIN photo-detector (PDA55) placed in the lens L_3 focal plane (Fig. 1). To evaluate the level of intensity scintillations in the channel we examined the received signal from a continuously running laser with a steady output intensity. An example of the received signal fluctuations,

measured by the PIN photo-detector, amplified by the low-noise preamplifier (SR560 with a gain of 20), and then acquired with sampling rate 1000 samples/sec, is presented in Fig. 2a.

The received signal standard deviation normalized by the mean value is as high as 0.8-0.9, which is indicative of a *strong scintillation regime* [10]. The corresponding ensemble-averaged received signal power spectrum S_{P_R} is shown in Fig. 2b. In atmospheric optics, laser beam intensity scintillations are traditionally described in terms of the logarithm of the normalized intensity I (for a point receiver) or received power P (for finite receiver telescope): $\xi_I = \ln(I) - \ln\langle I \rangle$ or $\xi_P = \ln(P) - \ln\langle P \rangle$, where $\langle I \rangle$ and $\langle P \rangle$ are ensemble (time) averaged values [10, 12]. A histogram that represents the distribution of the values of random variable ξ_P normalized by the total number of samples N , is shown in Fig. 3. Representing an approximation of the received power probability distribution, the histogram in Fig. 3 closely matches the log-normal distribution expected from theory [10].

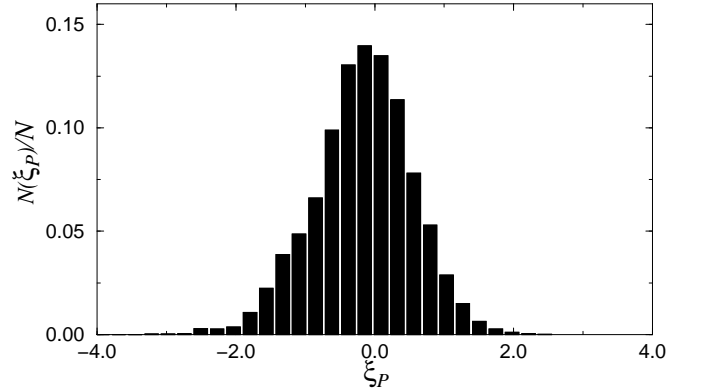


FIG. 3: Histogram of the probability distribution for the random variable $\xi_P = \ln(P/\langle P \rangle)$ measured by the PIN photo-detector. This histogram, $N(\xi_P)/N$, is computed using $N = 10^5$ consecutive samples of the data $P(t)$, a 20 sec fragment of which is shown in Fig. 2.

In the experiment with chaotic transceiver the laser generated a chaotic sequence of short-term ($\sim 1.0\mu s$) on-off pulses of intensity $U(t) = \sum_{j=0}^{\infty} w(t - t_j)$. Here $w(t - t_j)$ represents the waveform of an individual short-term rectangular pulse generated at the moment of time $t_j = t_0 + \sum_{n=0}^j T_n$, where T_n is the chaotic time interval between the n th and the $(n - 1)$ th pulse. The laser pulses were triggered by a TTL pulse signal from the chaotic transceiver controller CPPM Tx (see Fig. 1). The chaotic sequence of the time intervals $\{T_n\}$ corresponds to iterations of a chaotic process with the binary information signal added to the chaotic signal. This method of chaos communication is referred to as Chaotic Pulse Position Modulation (CPPM) [13]. Since both chaos and information are in the timing of the pulses, the particular intensity waveform of the generated light pulses is of

little consequence.

In the communication system discussed here the chaos is produced by iterations of a one-dimensional tent map (see [13] for details of the hardware design). Time intervals in the generated pulse sequence can be represented in the form of the following iterative map:

$$T_n = F(T_{n-1}) + d + mS_n, \quad (1)$$

where $F(\cdot)$ is a nonlinear function of the tent map and S_n is the binary information signal equal to either zero or one. The parameter m characterizes the modulation amplitude whereas the parameter d is a constant time delay needed for the practical implementation. The nonlinear function $F(\cdot)$ and parameters d and m were tuned to achieve a robust regime of the map's chaotic behavior. The interpulse intervals $\{T_n\}$ fluctuated chaotically ranging from $10\mu\text{sec}$ to $25\mu\text{sec}$ and supported a ~ 60 kbit per sec bit-rate.

The distorted chaotic pulses $U'(t)$ received at the PIN photo detector are applied to CPPM Rx (see Fig. 1). Due to the channel distortions and filtering in the PIN detector the received pulses become of bell-shaped waveform. Each received pulse triggered a timer circuit in CPPM Rx, when its amplitude exceeded a certain threshold level, and the receiver acquired two consecutive time intervals T_{n-1} and T_n . The information signal was recovered from the chaotic iterations $\{T_n\}$ using formula [14]:

$$mS_n = [T_n - F(T_{n-1}) - d]. \quad (2)$$

Since the chaotic decoder map in the receiver is matched to the encoder map in the corresponding transmitter, the time of the next arriving pulse can be predicted (see Eq.(1)). To improve system performance by reducing the probability of the channel noise falsely triggering the decoder, the input of the synchronized receiver was blocked until the moment of time when the next pulse was expected [13].

Due to the effects of atmospheric turbulence the received pulses were highly distorted. To illustrate, Fig. 4a shows the received pulse amplitude A_p as a function of time. Despite the severe pulse amplitude fluctuations clearly visible in Fig. 4a, the pulse propagation time τ_m , which is measured between the leading front of the TTL pulse applied to the laser and the maximal point of the received pulse, varied only within a 0.2μ sec time interval, see Fig.4b. Small fluctuations of the propagation time in the turbulent channel is a potential for very good performance of CPPM communication method. However, CPPM Rx is triggered when the leading front of the received bell-shaped pulse waveform crosses the threshold level. This level (~ 200 mV) was selected to minimize instances of receiver controller triggering caused by noise, or by pulses originating from local pulse reflections off nearby optical surfaces. Therefore, the actual delay time τ_t , measured between the leading front

of TTL pulses generated by CPPM Tx and the moments of CPPM Rx triggering, depends on the amplitude of the received pulses and fluctuates, see Fig. 4c. Gaps in the plots of τ_m and τ_t data occur due to the pulse amplitude fading when the pulse amplitude falls to the photo-receiver noise level and below threshold level, respectively. Although τ_t changes with the amplitude variation these changes remain less than the modulation amplitude $m \sim 1.5\mu\text{sec}$, see Eq. (1). Slow and small variation in the pulse propagation time is the key for CPPM controller self-synchronization, and hence for stability of the entire communication link.

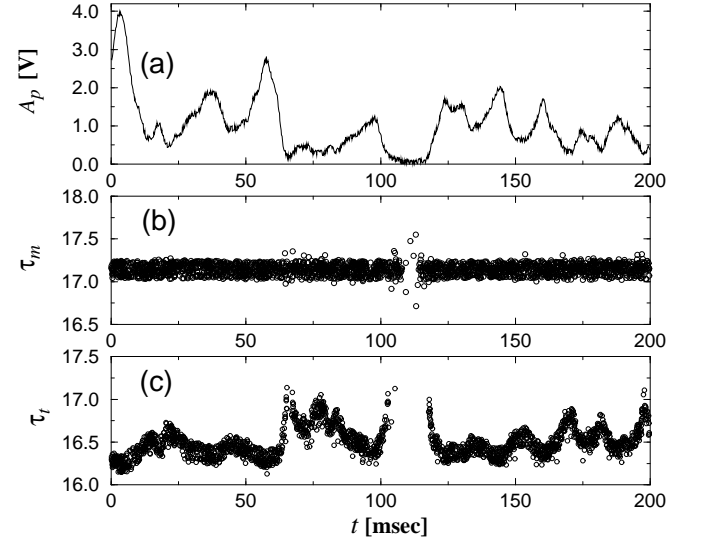


FIG. 4: Fluctuations of the CPPM pulses of light intensity after traveling through atmospheric turbulence. Pulse amplitude A_p measured in volts at the output of amplifier - (a). Propagation times τ_m - (b) and τ_t - (c) in μsec . The pulse propagation times are computed from data acquired simultaneously at the output of CPPM Tx and output of Amplifier (SR560) at a sampling rate of 5×10^6 samples per sec.

The dynamics of errors caused by the atmospheric turbulence was studied in the regime of real time transmission of binary pseudo-random code data. An example of a map of the lost data in such a transmission is presented in Fig. 5. The total Bit-Error-Rate measured in the experiment is 1.92×10^{-2} . From the detailed analysis of the error structure we conclude that main contributions to the BER are as follows. First, the loss of bits carried by the pulses which did not trigger the CPPM receiver due to the fading in the channel contributes $\sim 1.78 \times 10^{-2}$ to the BER ($\sim 92.7\%$). The fading moments occur randomly during the communication and cause the drop outs of blocks of data up to 1000 consecutive bits. The second group of errors occurs in the relatively short time intervals right before and after the failure of communication by fading. In these time intervals the amplitude of the received pulses is still close to the threshold and,

as consequence, even small noise in the channel can result in significant fluctuation of the interpulse intervals (see Fig. 4c). This effect contributes $\sim 1.4 \times 10^{-3}$ to the BER ($\sim 7.3\%$). These two fading related error contributions would cause data loss not only in this *chaos* based communication system but would equally affect a similar type of *periodic* pulse position system. The rest of the errors which are not related to the complete failure of the channel by the fading instances and can therefore be associated with the susceptibility of the *chaos* communication to the channel distortions contributed to the BER only $\sim 5.5 \times 10^{-5}$.

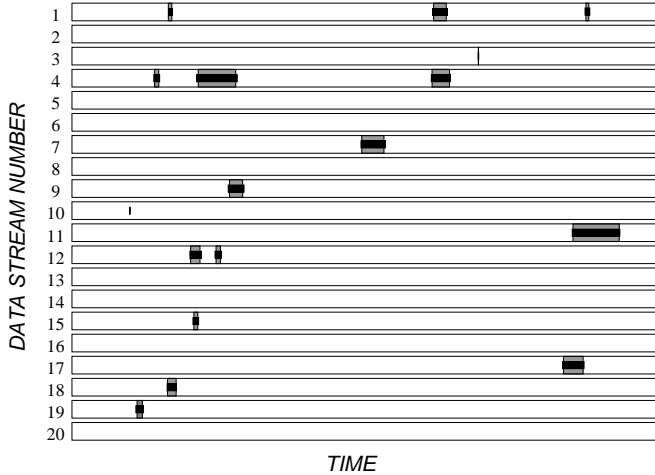


FIG. 5: Typical structure of errors shown in 20 consecutive measured data streams each of length ~ 170 msec transmitted at ~ 2 min intervals. Each strip presents 10000 bits which are transmitted with the CPPM method. White intervals of the strips mark blocks of data received without errors. Narrow black ribbons in the middle of strips mark the blocks of the data received with errors. The gray background shows the blocks of the dropped out data caused by the loss of CPPM pulses due to fading instances.

This structure of errors indicates that the CPPM communication method supports robust communications over the turbulent channel except for the time intervals when the channel fails due to fading. Thanks to the self-synchronizing feature of this chaos communication method after the total fading phase is over the CPPM receiver re-synchronizes fast. In fact it needs to receive only two correct pulses to establish the regime of chaos synchronization (see [13] for details).

The authors are grateful to L.S. Tsimring, H.D.I. Abarbanel, L. Larson, and A.R. Volkovskii for helpful discussions. This work was supported in part by U.S. Department of Energy (grant DE-FG03-95ER14516), the U.S. Army Research Office (MURI grant DAAG55-98-1-0269). The authors also thank J. Gowens and J. Carrano for support in the development of the Atmospheric Laser

Optics Testbed (A LOT) at Adelphi, Maryland used in the experiments.

-
- [1] K. M. Cuomo and A.V. Oppenheim, Phys. Rev. Lett. **71**, 65 (1993); L. Kocarev *et al*, Int. J. Bif. Chaos, **2**, 709 (1992); T. L. Carroll and L. M. Pecora, IEEE Trans. Circuits Syst. **40**, 646 (1993); T.L. Carroll, Phys. Rev. E **53**, 3117 (1996); C. W. Wu and L. O. Chua Int. J. Bif. Chaos **3**, 1619 (1993)
 - [2] P. Colet and R. Roy, Opt. Lett **19**, 2056 (1994); P. Celka, IEEE Trans. Circuits Syst. **42**, 455 (1995); IEEE Trans. Circuits Syst. **43**, 869 (1996); C. R. Mirasso, P. Colet, and P. Garcia-Fernández, Photonics Technol. Lett. **8**, 299 (1996); G. D. VanWiggeren and R. Roy, Science **279**, 1198 (1998); Phys. Rev. Lett. **81**, 3547 (1998); H. D. I. Abarbanel and M. B. Kennel, Phys. Rev. Lett. **80**, 3153 (1998).
 - [3] H. Fujisaka and T. Yamada, Prog. Theor. Phys. **69**, 32 (1984); L. M. Pecora and T. L. Carroll, Phys. Rev. Lett. **64**, 821 (1990);
 - [4] D. R. Frey, IEEE Trans. Circuits Syst. **40**, 646 (1993); A. R. Volkovskii and N. F. Rulkov, Tech. Phys. Lett. **19**, 97 (1993); U. Feldman, M. Hasler, and W. Schwarz, Int. J. Circuit Theory Appl. **24**, 551 (1996); L. Kocarev and U. Parlitz, Phys. Rev. Lett. **74**, 5028 (1995).
 - [5] See, for example, special focus issues: IEEE Trans. Circuits Syst. **48** No. 12 (2001); Chaos **6** No. 3 (1996); Chaos **7** No. 4 (1997); Int. J. Bif. Chaos **10**, No. 11&12 (1993); Int. J. Circuit Theory Appl. **27** (1999);
 - [6] G. Kolumban, M. P. Kennedy and L. O. Chua, IEEE Trans. Circuits Syst. **45**, 1129 (1998); C. Williams, IEEE Trans. Circuits Syst. **48**, 1394 (2001).
 - [7] T. L. Carroll, Phys. Rev. E **53** 3117 (1996); T. L. Carroll and G. A. Johnson, Phys. Rev. E **57** 1555 (1998); E. Rosa, S. Hayes, and C. Grebogi, Phys. Rev. Lett. **78** 1247 (1997); H. Torikai, T. Saito, and W. Schwartz, IEEE Trans. Circuits Syst. **46**, 1072 (1999).
 - [8] T. L. Carroll, IEEE Trans. Circuits Syst. **42**, 105 (1995); IEEE Trans. Circuits Syst. **48**, 1519 (2001); N. F. Rulkov and L. Tsimring, Int. J. Circuit Theory Appl. **27**, 555 (1999);
 - [9] Yu. A. Kravtsov, em Appl. Optics, **32**, 2681 (1993).
 - [10] L. C. Andrews, R.L. Phillips, and C.Y. Hopen, *Laser Beam Scintillation with Applications*, (SPIE Press, Bellingham, 2001).
 - [11] Yu. A. Kravtsov and A.I. Saichev, *Sov. Phys. Usp.*, **25**, 494 (1982).
 - [12] S. M. Rytov, Yu. A. Kravtsov, and V. I. Tatarskii *Principles of Statistical Radiophysics 4, Wave Propagation through Random Media*, (Springer-Verlag, Berlin, 1989).
 - [13] M. M. Sushchik, *et al. IEEE Communication Letters*, **4**, 128 (2000); N. F. Rulkov, *et al. IEEE Trans. Circ. Syst.* **48**, 1436 (2001).
 - [14] In the CPPM Tx and CPPM Rx devices the consecutive values of T_n and T_{n-1} are generated and stored in the form of voltage signals. Eqs. (1) and (2) are implemented using an analog electrical circuit of the nonlinear function $F(\cdot)$ and a subtracting circuit, see Ref. [13] for details.